HHS Public Access

Author manuscript

Proc SPIE Int Soc Opt Eng. Author manuscript; available in PMC 2017 October 06.

Published in final edited form as:

Proc SPIE Int Soc Opt Eng. 2017 March ; 10132: . doi:10.1117/12.2255695.

High-resolution extremity cone-beam CT with a CMOS detector: Task-based optimization of scintillator thickness

Q. Cao[a], **M. Brehler**[a], **A. Sisniega**[a], **J. W. Stayman**[a], **J. Yorkston**[b], **J. H. Siewerdsen**[a,c], and **W. Zbijewski**[a]

[a]Department of Biomedical Engineering, Johns Hopkins University, Baltimore, MD USA 21205

[b]Carestream Health, Rochester, NY USA

[c]Russell H. Morgan Department of Radiology, Johns Hopkins University, Baltimore, MD USA 21287

Abstract

Purpose—CMOS x-ray detectors offer small pixel sizes and low electronic noise that may support the development of novel high-resolution imaging applications of cone-beam CT (CBCT). We investigate the effects of CsI scintillator thickness on the performance of CMOS detectors in high resolution imaging tasks, in particular in quantitative imaging of bone microstructure in extremity CBCT.

Methods—A scintillator thickness-dependent cascaded systems model of CMOS x-ray detectors was developed. Detectability in low-, high- and ultra-high resolution imaging tasks (Gaussian with FWHM of ~250 μm, ~80 μm and ~40 μm, respectively) was studied as a function of scintillator thickness using the theoretical model. Experimental studies were performed on a CBCT test bench equipped with DALSA Xineos3030 CMOS detectors (99 μm pixels) with CsI scintillator thicknesses of 400 μm and 700 μm, and a 0.3 FS compact rotating anode x-ray source. The evaluation involved a radiographic resolution gauge (0.6–5.0 lp/mm), a 127 μm tungsten wire for assessment of 3D resolution, a contrast phantom with tissue-mimicking inserts, and an excised fragment of human tibia for visual assessment of fine trabecular detail.

Results—Experimental studies show ~35% improvement in the frequency of 50% MTF modulation when using the 400 μm scintillator compared to the standard nominal CsI thickness of 700 μm. Even though the high-frequency DQE of the two detectors is comparable, theoretical studies show a 14% to 28% increase in detectability index (d'^2) of high- and ultrahigh resolution tasks, respectively, for the detector with 400 μm CsI compared to 700 μm CsI. Experiments confirm the theoretical findings, showing improvements with the adoption of 400 μm panel in the visibility of the radiographic pattern (2× improvement in peak-to-through distance at 4.6 lp/mm) and a 12.5% decrease in the FWHM of the tungsten wire. Reconstructions of the tibial plateau reveal enhanced visibility of trabecular structures with the CMOS detector with 400 μm scinitllator.

wzbijewski@jhu.edu; phone 410-955-1319; fax 410-955-9826;.

Conclusion—Applications on CMOS detectors in high resolution CBCT imaging of trabecular bone will benefit from using a thinner scintillator than the current standard in general radiography. The results support the translation of the CMOS sensor with 400 μm CsI onto the clinical prototype of CMOS-based extremity CBCT.

Keywords

cone-beam CT; extremities imaging; CMOS; scintillator thickness; bone microarchitecture

1. INTRODUCTION

CMOS x-ray detectors offer lower electronic noise, smaller pixel sizes and faster frame rates than a:Si Flat-Panel Detectors (FPDs). These advantages are likely to benefit high resolution applications, for example mammography and digital breast tomosynthesis [1,2] and quantitative imaging of trabecular bone. The capability for *in vivo* evaluation of trabecular detail could significantly enhance clinical applications of the recently introduced extremities CBCT systems [3,4]. Changes in bone microstructure are a potential early indicator of osteoporosis and osteoarthritis (where alterations in subchondral bone are hypothesized to precede cartilage degeneration [5]). However, accurate assessment of metrics such as trabecular thickness and trabecular spacing requires resolving <100 μm details and is thus typically performed *ex vivo* with microCT as the gold standard [6]. High-resolution peripheral quantitative CT (HR-pQCT) was developed with resolution that has been shown to be sufficient for quantitative measurements of trabecular microarchitectures, but exhibits somewhat limited field-of-view and long scan times [7]. Among the current clinical orthopedic imaging modalities, FPD-based CBCT is promising for applications in *in vivo* assessment of bone structure because of the small pixel size of FPDs (approx. 130–190 μm). The robustness of quantitative measurements obtained using extremities CBCT would however benefit from further increase in spatial resolution.

The resolution of extremity CBCT can be improved to achieve improved visualization of trabecular detail through adoption of novel CMOS detectors. Theoretical simulation studies and benchtop experimentation confirmed the benefits of CMOS detectors over FPDs in extremity CBCT, including ~2× increased detectability of high-frequency tasks and improved correlation with gold-standard micro-CT in the metrics of trabecular structure [8]. Fig. 1 illustrates the advantages of smaller pixel size in studies comparing an FPD (Varian PaxScan 4030CB, 194 μm pixels) to a CMOS x-ray detector (Dalsa Xineos3030, 99 μm pixels). Both scans were obtained in a geometry emulating that of an extremities CBCT system. Reconstructions of cadaveric ulna are compared to gold standard micro-CT. Improved resolution and delineation of trabecular detail is apparent for CMOS-based CBCT. This is further confirmed in improved agreement of trabecular segmentation obtained with Otsu's method, as evaluated using Dice coefficient for 25 regions-of-interest (ROIs) in the ulna. More accurate segmentation yields improved performance in the metrics of bone microarchitecture: CMOS-based CBCT was found to exhibit better correlation with micro-CT in measurements of bone volume in the same set of 25 ulnar ROIs (correlation coefficient r=0.9 for CMOS vs. 0.6 for FPD) and trabecular spacing (r=0.8 for CMOS vs. 0.6 for FPD).

In this work, we focus on optimization of the scintillator thickness for CMOS applications in extremity CBCT. Despite their smaller pixel size, the CMOS sensors often utilize scintillators of similar thickness as those employed in FPDs for general radiography (~600–700 μm). We use a theoretical cascaded systems model of CMOS detectors to investigate the tradeoffs in noise and resolution as a function of scintillator thickness for a variety of tasks in orthopedic imaging, in particular high-resolution tasks representative of fine trabecular detail. A custom CMOS detector with 400 μm CsI thickness is experimentally evaluated in comparison to a standard 700 μm sensor under identical imaging conditions using a flexible test-bench setup (Fig. 2). The results of the theoretical and experimental studies guided the development of a clinical prototype of a CMOS-based extremity CBCT scanner to be deployed in pilot clinical studies in *in-vivo* imaging of bone health. A prototype scanner based on the gantry of the current FPD-based extremities CBCT was constructed and is anticipated to enter pre-clinical evaluation this year.

2. METHODS

2.1 Task-based optimization of CMOS scintillator thickness

Task-based investigation of the effects of scintillator thickness was performed using a 7-stage cascaded systems model [9] of a CMOS detector. Novel contributions compared to existing cascaded models of FPDs included (i) an additional stochastic blurring stage simulating the adhesive layer between the scintillator assembly and the CMOS [8] (in FPDs the scintillator is often deposited directly on the FPD) and (ii) thickness dependent scintillator blurring (T_3). To parameterize the model, measurements of dark signal, signal/exposure, Noise Power Spectrum (NPS) and Modulation Transfer Function (MTF) were performed using an experimental test bench (Fig. 2) on two CMOS panels (Xineos3030, Teledyne DALSA, NL), both with 99 μm pixel size: one with a standard 700 μm CsI scintillator (nominal thickness in production units), and one custom sensor with 400 μm thick CsI. (see Sec. 2.2). In particular, the thickness-dependent scintillator blur T_3 was estimated from the measured detector MTFs by dividing by a product of the K-fluorescence, optical adhesive and pixel aperture blurs computed from the model. This empirically determined T_3 was fit with a function of the form:

$$T_3(u)=A\exp(-|u|/B)+(1-A)/(1+Hu^2) \quad (1)$$

where u is spatial frequency and H is a depth dependent variable, so that the Lorenzian term describes thickness-dependent blur of the structured CsI:Tl crystals (the exponential term accounts for the thin homogeneous layer of CsI:Tl deposited on the surface of the structured crystals [10]). Parameter H was fit to a parabola as a function of scintillator thickness. Parameters of the theoretical model are summarized in Table 1.

Evaluation of detector performance as a function of scintillator thickness employed the non-prewhitening detectability index:

$$(d'_{NPW})^2 = \frac{\left[\int\int_{-f_{Nyq}}^{f_{Nyq}} MTF^2 \cdot W_{task}^2 \, dudv\right]^2}{\int\int_{-f_{Nyq}}^{f_{Nyq}} NNPS \cdot MTF^2 \cdot W_{task}^2 \, dudv} \quad (2)$$

where u and v and spatial frequencies, and *MTF* and normalized NPS (*NNPS*) are thickness-dependent functions obtained from the cascaded systems model. Three tasks were considered (Fig. 3): (i) a low-resolution task, corresponding to a Gaussian blob in the radiographic projection with FWHM = 250 μm, (ii) a high resolution task (FWHM = 83 μm, corresponding to the typical trabecular spacing), and (iii) an ultra-high-resolution task (FWHM = 41 μm). The modelling was performed for a simulated 90 kVp beam (+0.2 mm Cu) attenuated by a digital knee phantom consisting of 8 cm water, 7.6 cm spongiosa and 0.4 cm cortical bone. For simplicity, the analysis was performed in the 2D radiographic projection domain. Trends evident from the 2D model remain valid in extension to the 3D reconstruction cascade [11] due in part to the linearity of filtered backprojection and differing only in 3D sampling effects.

2.2 Experimental validation

Imaging studies were performed on a CMOS CBCT test bench (Fig. 2) in the geometry of the extremity CBCT system (SAD=380 mm, SDD=530 mm). A 0.3 FS compact rotating anode x-ray source with 3 kW maximal power (IMD RTM 37, IMD, IT) was used. As mentioned in Sec. 2.1, two DALSA Xineos 3030HR CMOS detectors with different nominal scintillator thicknesses (700 μm and 400 μm) were both evaluated on the bench. Imaging studies involved a resolution gauge (Gammex 07–538, 0.6–5.0 lp/mm) for assessment of 2D resolution, a ~127 μm tungsten wire tensioned within a hollow plastic cylinder for measurement of 3D resolution (wire phantom), and a water-equivalent cylinder with embedded tissue-mimicking inserts (Gammex 467) for studies of contrast-to-noise ratio (CNR) in 3D reconstructions (contrast phantom). Visual evaluation of clinical image quality was performed with an excised fragment of human tibial plateau.

The resolution gauge was placed on the surface of each detector. 200 frames were acquired at ~68% detector saturation, gain and offset corrected and averaged to reduce noise. Twenty line profiles perpendicular to the line patterns were averaged. Modulation for each line-pair pattern was characterized by peak-to-trough difference in the profiles. The CBCT scans of the wire phantom, the contrast phantom and the tibial plateau all involved 720 projections acquired over 360°. The scan techniques were varied between 0.06 mAs to 0.184 mAs per projection, corresponding to central CTDI doses of 12 to 38 mGy (typical dose in extremity CBCT is ~12 mGy). High-resolution reconstructions of the wire phantom and the tibial plateau employed the Feldkamp (FDK) algorithm with 25 μm voxels and a ramp filter with a cutoff at the Nyquist. The contrast phantom was reconstructed with a “soft-tissue” protocol with 2×2 pixel binning, 325 μm voxels and a Hann filter with cutoff at 0.7× Nyquist frequency.

3. RESULTS AND BREAKTHROUGH WORK

Fig. 4 compares the measured MTF for the CMOS detectors with 400 μm and 700 μm CsI. The thinner scintillator yields 37.5% imporvement in MTF_{50} and 37.0% improvement in MTF_{20}. Results of the cascaded system analysis are also shown, both at the two thicknesses where measurements were available and at intermediate thicknesses where the thickness-dependent T_3 model was used to predict the MTF. Good agreement was also obtained between the theoretical prediction and the measured DQE. Due to the better quantum efficiency of the thicker detector, low-frequency DQE for the CMOS with 700 μm CsI was found to be better than that of the thinner scintilator. Moreover, despite the superior high frequency MTF of the thinner scinillator, the DQE of the two detectors converges at high frequencies. Analysis of detectability provides an insight into whether the improved MTF of the thin scintillator is sufficient to enhance the conspicuity of high resolution features, even though there is no gain in DQE.

Fig. 5 shows the detectability index for CMOS detectors with various CsI thicknesses, normalized to that of the detector with 700 μm scintillator (representing the nominal value in CMOS and FPD panels for general radiography). For the low-resolution task, the 700 μm scintillator achieves optimal detectability among the CsI thicknesses examined in this study. For the high- and ultra-high resolution tasks, however, the reduced blur offered by thinner scintillators leads to an improvement in detectability compared to the 700 μm scintillator. For 400 μm CsI, the detectability is increased compared to 700 μm CsI by 1.14× for the high resolution task and 1.28× for the ultra-high resolution task. The shift towards thinner optimal scintillator thicknesses is less pronounced between the high-resolution and ultra-high resolution tasks (optimized at ~400 μm CsI and ~350 μm CsI, respectively) than between the low-resolution task and the high-resolution task, indicating diminishing returns from using scintillators even thinner than ~300 μm CsI due to their reduced quantum efficiency.

Experimental results corroborate the theoretical findings. In the bar phantom (Fig. 6A–B), peak-to-trough transmissivity values of 0.071, 0.054 and 0.051 were achieved using CMOS with 400 μm CsI for line patterns at 4, 4.3, 4.6 lp/mm, respectively. The CMOS with 700 μm CsI only attained peak-to-through values of 0.0374, 0.0306 and 0.0235. Furthermore, the CMOS with 400 μm CsI was able to resolve the line pair pattern at 5 lp/mm (approaching the Nyquist frequency of detector pixels), which was not possible with the 700 μm scintillator. The advantage of the thinner scintillator is also apparent in 3D reconstructions of the wire phantom (Fig. 6C). A Gaussian was fit to the central profiles of the wire, yielding an FWHM of 0.24 mm for CMOS with 400 μm CsI, compared to 0.21 mm for the panel with thicker CsI. While the improved spatial resolution achieved using a thinner scintillator comes at the price of increased noise and reduced detectability for low-frequency tasks, the CNR for contrast levels of interest in orthopedic imaging remains high. Evaluation of the reconstructions of the contrast phantom found that at a dose level matched to the current extremity CBCT, the CNR for inner bone (230 HU), adipose (−100 HU) and liver (80 HU) are 14.1, 3.6 and 6.7, respectively, for the CMOS with 700 μm CsI, and 10.7, 2.7 and 4.6 for the detector with 400 μm CsI.

Reconstructions of human tibial plateau are shown in Fig. 7. The CMOS detector with thinner scintillator achieves improved delineation of the edges of the bone and better overall modulation of the trabecular pattern. This is particularly apparent in the magnified views of the peripheral area of the bone, where a very fine cancellous matrix is present.

4. CONCLUSIONS

The theoretical and experimental studies confirm the benefits of using a scintillator thinner than the current industrial standard in CMOS detectors developed for high resolutions tasks in orthopedic imaging. The fact that better performance was achieved with the 400 μm scintillator despite the comparable high-frequency DQE of the sensors with 400 μm and 700 μm CsI suggests that the improved MTF of the 400 μm CsI plays a stronger role in determining the performance in the high-frequency tasks than the increased noise. Moreover, agreement between theoretical and experimental studies indicates that this finding is not merely an artifact of choosing the NPW observer model in the detectability calculation. While the application of the thinner scintillator results in ~20% reduction in the detectability in low frequency tasks (“soft-tissue” imaging), the experimental studies show that the CMOS detector with 400 μm scintillator maintains sufficiently high CNR for tissues of interest in extremity CBCT.

Further validation of the potential advantages of the CMOS detector with 400 μm scintillator are underway, focusing on assessment of performance in quantitative metrics of trabecular structure compared to gold standard micro-CT. Translation of the CMOS-based imaging chain onto the CBCT gantry is ongoing, with anticipated deployment in pilot clinical studies within ~1 year. Through the application of an optimized CMOS sensor and novel deblurring and motion correction algorithms [12,13], this new generation of extremity CBCT will provide a comprehensive platform for in-vivo assessment of bone health at spatial scales ranging from gross morphology to trabecular microarchitecture.

Acknowledgments

Work supported by NIH Grant R01-EB-018896.

References

1. Konstantinidis, AC., Szafraniec, MB., Speller, RD., Olivo, A. Nucl Instruments Methods Phys Res Sect A Accel Spectrometers, Detect Assoc Equip. Vol. 689. Elsevier; 2012. The Dexela 2923 CMOS X-ray detector: A flat panel detector based on CMOS active pixel sensors for medical imaging applications; p. 12-21.
2. Zhao, C., Konstantinidis, AC., Zheng, Y., Anaxagoras, T. Phys Med Biol. Vol. 60. IOP Publishing; 2015. 50 μm pixel pitch wafer-scale CMOS active pixel sensor x-ray detector for digital breast tomosynthesis; p. 8977
3. Tuominen EKJ, Kankare J, Koskinen SK, Mattila KT. Weight-bearing CT imaging of the lower extremity. AJR Am J Roentgenol. 2013; 200(1):146–148. [PubMed: 23255755]
4. Carrino JA, Al Muhit A, Zbijewski W, Thawait GK, Stayman JW, Packard N, Senn R, Yang D, Foos DH, et al. Dedicated cone-beam CT system for extremity imaging. Radiology. 2014; 270(3):816–824. [PubMed: 24475803]
5. Weinans, H., Siebelt, M., Agricola, R., Botter, SM., Piscaer, TM., Waarsing, JH. Bone. Vol. 51. Elsevier Inc; 2012. Pathophysiology of peri-articular bone changes in osteoarthritis; p. 190-196.

6. Roberts BC, Thewlis D, Solomon LB, Mercer G, Reynolds KJ, Perilli E. Systematic mapping of the subchondral bone 3D microarchitecture in the human tibial plateau: Variations with joint alignment. J Orthop Res. 2016
7. Nishiyama KK, Shane E. Clinical imaging of bone microarchitecture with HR-pQCT. Curr Osteoporos Rep. 2013; 11(2):147–155. [PubMed: 23504496]
8. Cao Q, Brehler M, Sisniega A, Marinetto E, Zyazin A, Peter I, Stayman J, Yorkston J, Siewerdsen J, et al. High-resolution cone-beam CT of the extremities and cancellous bone architecture with a CMOS detector. AAPM Annu Meet. 2016; 3797
9. Siewerdsen JH, Antonuk LE, El-Mohri Y, Yorkston J, Huang W, Boudry JM, Cunningham Ia. Empirical and theoretical investigation of the noise performance of indirect detection, active matrix flat-panel imagers (AMFPIs) for diagnostic radiology. Med Phys. 1997; 24(1):71. [PubMed: 9029542]
10. Zhao W, Ristic G, Rowlands J. X-ray imaging performance of structured cesium iodide scintillators. Med Phys. 2004; 31:2594–2605. [PubMed: 15487742]
11. Tward DJ, Siewerdsen JH. Cascaded systems analysis of the 3D noise transfer characteristics of flat-panel cone-beam CT. Med Phys. 2008; 35(12):5510. [PubMed: 19175110]
12. Tilley, S., Siewerdsen, J., Stayman, J. Phys Med Biol. Vol. 61. IOP Publishing; 2016. Model-based iterative reconstruction for flat-panel cone-beam CT with focal spot blur, detector blur, and correlated noise; p. 296
13. Sisniega A, Stayman JW, Cao Q, Yorkston J, Siewerdsen JH, Zbijewski W. Image-based motion compensation for high-resolution extremities cone-beam CT. Proc SPIE. 2016; 9783:97830K.

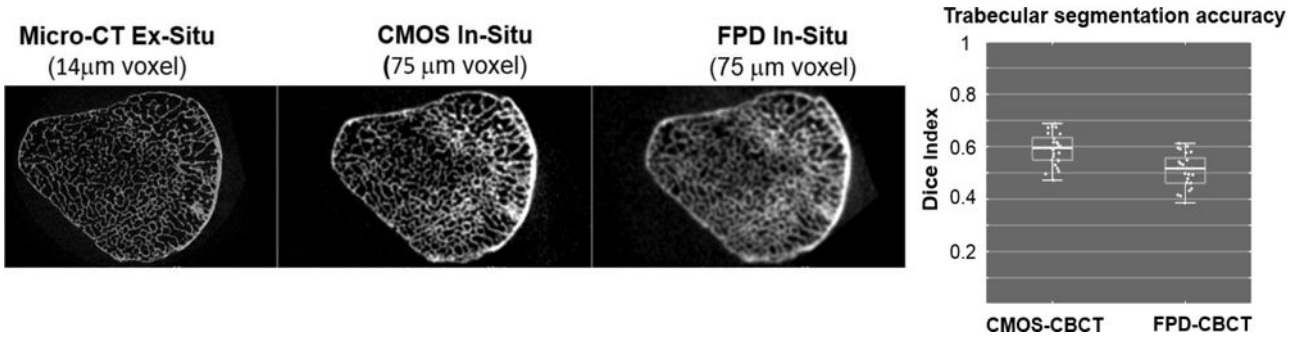

Figure 1.

Comparisons of the visualization of trabecular detail in cadaveric ulna using gold-standard micro-CT, CMOS-bases CBCT with 100 μm pixels and FPD-based CBCT with 194 μm pixels. CMOS-based CBCT achieves improved segmentation of the trabeculae, as measured using Dice coefficient against micro-CT.

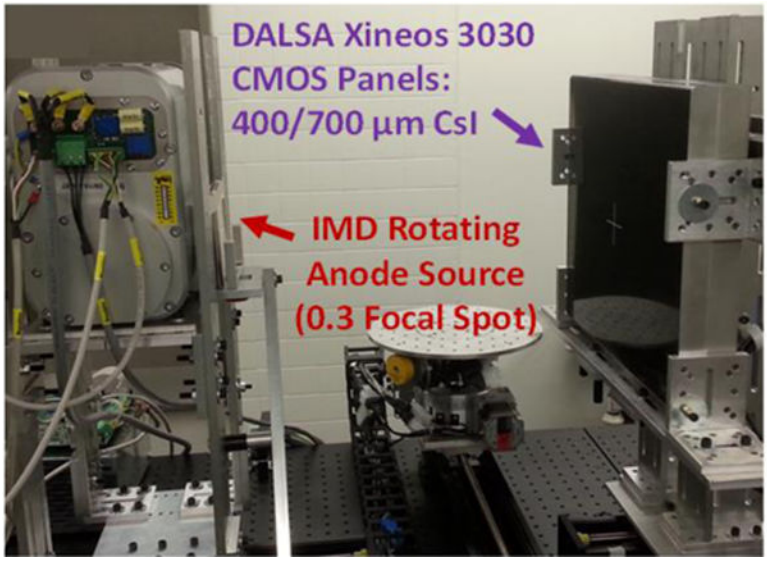

Figure 2.
CBCT test bench setup with a CMOS detector (30 cm × 30 cm) and a small focal spot source. In this work, benchtop experimentation and task-based performance modelling were used to determine optimal CMOS scintillator thickness for applications in extremity CBCT imaging, in particular in quantitative assessment of trabecular architecture.

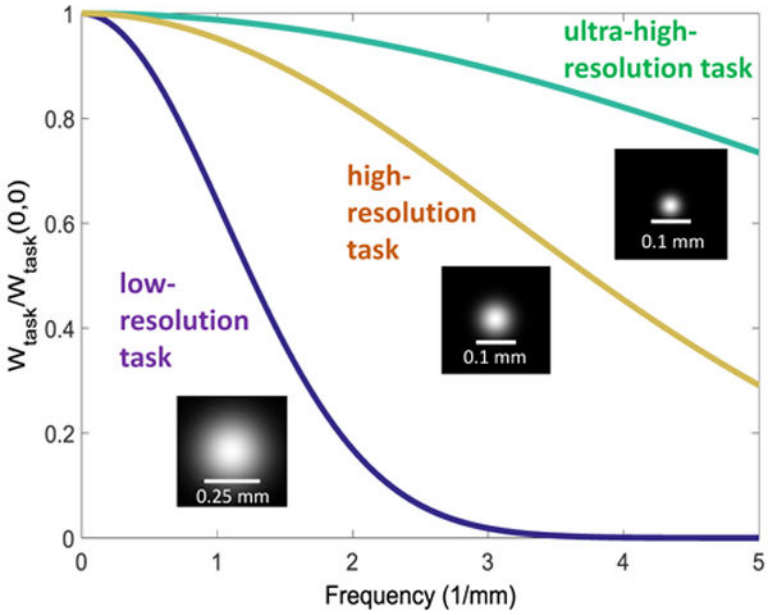

Figure 3.

Task functions used in the analysis. Low resolution task, high resolution task and ultra-high-resolution task represents detection of soft tissue, trabecular bone, and small trabecular fragments, respectively.

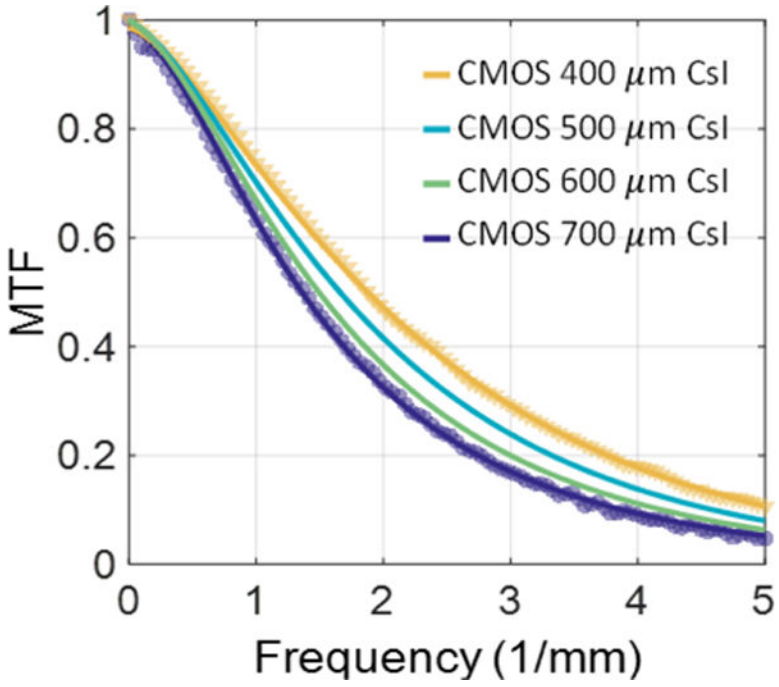

Figure 4.
Measured (markers) vs. modelled (lines) MTFs of CMOS detectors with 400 and 700 μm CsI, as well as the modelled MTF for intermediate thicknesses.

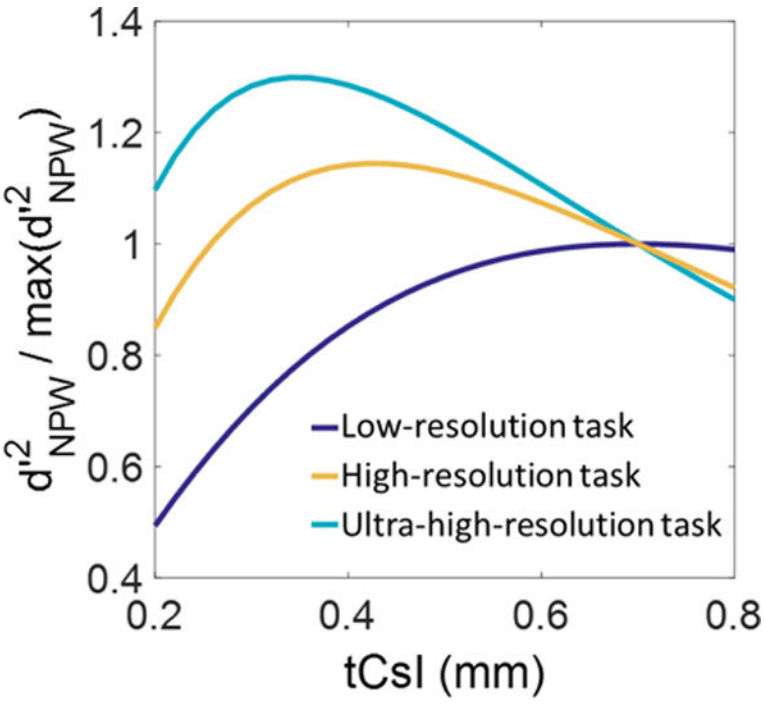

Figure 5.

Squared detectability as a function of scintillator thickness for the three tasks of Fig. 3. Detectabilities of each task are normalized to their value for the 700 μm scintillator, representative of thickness used in general radiography.

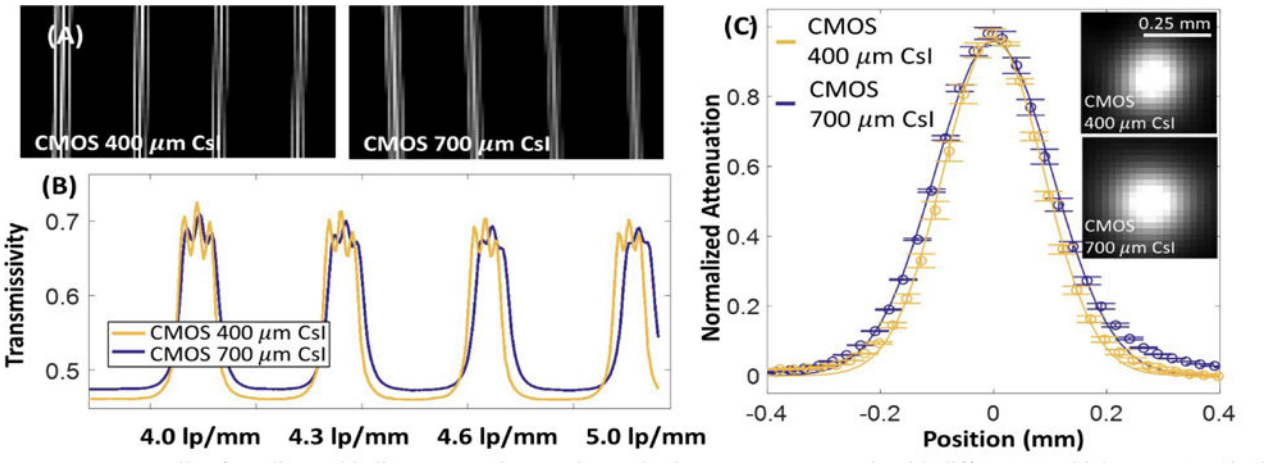

Figure 6.

(A) Details of a radiographic line pattern phantom imaged using two CMOS panels with different CsI thicknesses (nominal frequencies, from left to right: 4, 4.3, 4.6, 5 lp/mm). Average profiles though the line patterns are shown in **(B).** In **(C)**, reconstructions of the Tungsten wire phantom are compared for the two CMOS panels. The thinner scintillator achieves 12% improvement in FWHM.

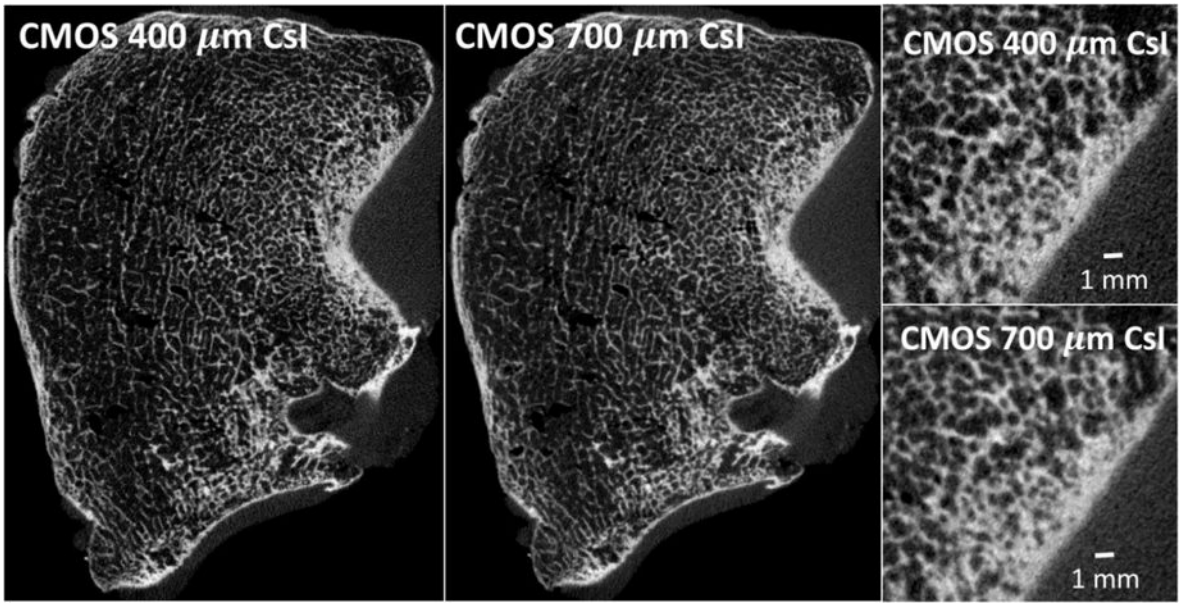

Figure 7.
Reconstructions of an excised human tibial plateau obtained with the two CMOS panels. The detector with 400 μm scintillator achieves better modulation of bone microstructure.

Table 1

Parameters of the cascaded systems model of CMOS x-ray detectors.

Detector Parameters	Values
Scintillator Thickness	400–700 μm
Packing Fraction	55%
Adhesive Thickness	20 μm
Optical Coupling Efficiency	0.27
K -fluorescence Probability	0.83
K -fluorescence Yield	0.87
Pixel Size	99 μm
Fill Factor	85%
Additive Noise	300 e^{-}